DOI: 10.48011/asba.v2i1.1007

# Model-Based Approach for Cornering Stiffness and Yaw Moment of Inertia Estimation of a Scaled Electric Vehicle ⋆

**Alexandre M. Ribeiro** * **André R. Fioravanti** *
**Ely C. de Paiva** *

* *Faculdade de Engenharia Mecânica - FEM, Universidade Estadual de Campinas - UNICAMP, SP. (e-mails: {amribeiro, fioravanti, elypaiva}@fem.unicamp.br)*

**Abstract:** This paper addresses the problem of estimating the tire cornering stiffness coefficient and the yaw moment of inertia of a scaled car-like vehicle. The method merges measurements information of the vehicle lateral response along with its nonlinear planar model. Aiming effective and accurate results, we propose solving an optimization problem based on a representative dataset obtained experimentally using a persistently exciting input. The validation of the proposed method is shown by comparing the agreement between numerical simulations, evaluated with the estimated parameters, with experimental data. Three representative maneuvers are considered for this purpose, including indoor and outdoor experiments.

*Keywords:* Parameter estimation; cornering stiffness; lateral vehicle dynamics; model-based parameter identification; vehicle dynamics.

## 1. INTRODUCTION

Tire cornering stiffness and yaw moment of inertia are two important parameters that strongly influence the vehicle motions. They are present in the majority of mathematical models that describe the vehicle lateral dynamics, ranging from the simplified linearized models to the nonlinear ones with higher complexity.

The standard approach that deals with parameter identification follows rigorous testing in a dedicated facility. These workstations provide a truthful dataset allowing an accurate identification. It is often an expensive and time-consuming approach (Matsubara et al., 2019).

Given the importance of these parameters, there are a number of works in literature intended to estimate those values based on different theoretical concepts.

In (Yang et al., 2017) and (Han et al., 2018), the cornering stiffness coefficient is estimated considering the linearized single-track vehicle model. The approach is solved numerically through a least square algorithm. In (Fnadi et al., 2019), a Kalman Filter that merges information about steering angle and inertial measurements is used. In (Zhang et al., 2015) a time-frequency analysis is presented considering a series of harmonic excitation. In (Denis et al., 2015), the cornering stiffness estimation is performed based on a gradient search algorithm.

⋆ The authors acknowledge the funding received from: FAPESP Regular project AutoVERDE N. 2018/04905-1, Ph.D. FAPESP 2018/05712-2, and Project INCT-SAC - Autonomous Collaborative Systems - (CNPq 465755/2014-3, FAPESP 2014/50851-0), FAPESP BEP (p. 2017/11423-0).

The objective of this paper is to experimentally demonstrate and apply a reliable algorithm for the estimation of the cornering stiffness coefficient and yaw moment of inertia. The proposed model-based method relies on measures obtained with ordinary sensors such as encoders, global positioning system (GPS), inertial measurement units (IMU), and encoders. Furthermore, in an attempt to capture the nonlinearities inherent to the vehicle response we propose using the nonlinear model instead of its linearized version.

The remaining sections of this paper are organized as follows. In Section 2, the motivations about the vehicle in the study are presented. Section 3 introduces the vehicle mathematical model. Section 4 shows the parameter identification method. In Section 5 the validation of the proposed method is illustrated by comparing the agreement between numerical simulations with experimental data and, finally, conclusions and directions for future work are provided in Section 6.

## 2. MOTIVATIONS

A four-wheeled scaled vehicle is used for the validation experiment. The platform, shown in Figure 1, has independent rear-wheel traction and a steering system that follows the Ackermann geometry. It is equipped with a collection of off-the-shelf sensors such as encoders, global positioning system, IMU, camera, and a Light Detection And Ranging (LIDAR). Moreover, the platform is large enough to host powerful onboard computing. See Nogueira et al. (2018) for a complete and comprehensive analysis of this prototype.

The motivation for using a scaled vehicle is grounded in the fundamental concept that it considerably simplifies the experimental validation task while keeping the same level

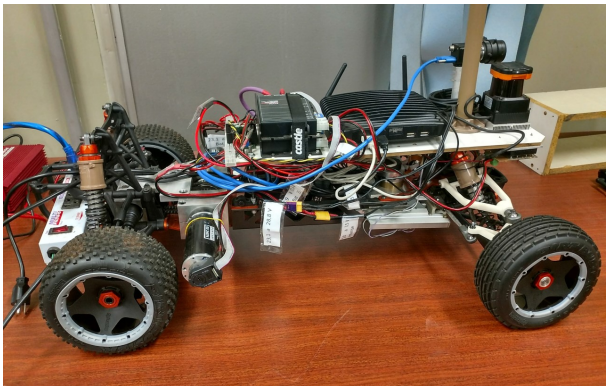

Figure 1. Four-wheeled 1:5-scale platform used in the experiments.

of sensing capabilities of a full-sized vehicle. Such scaled vehicles can serve as a testbed for validating experimental applications.

In literature, scaled vehicles are largely applied in diverse theoretical fields such as path planning (Pinto et al., 2019), dynamic response analysis (Kozłowski, 2019), rollover prevention (Treetipsounthorn and Phanomchoeng, 2018), and parameter identification (Polley et al., 2006).

Due to the need to identify the cornering stiffness and yaw moment inertia of the vehicle presented in Figure 1, we propose a scalable identification method using ordinary and conventional sensors. The main advantage expected from the proposed approach is that it can be extended to other projects with minimal efforts. To begin the design, we first present the vehicle mathematical model.

## 3. VEHICLE MODELING

To describe the vehicle dynamics, a nonlinear single-track model, also known as bicycle model (see Figure 2), is employed. This model assumes a single tire at each axle with twice the force capability of the individual tires. Additionally, it considers pure planar motion neglecting roll and pitch dynamics.

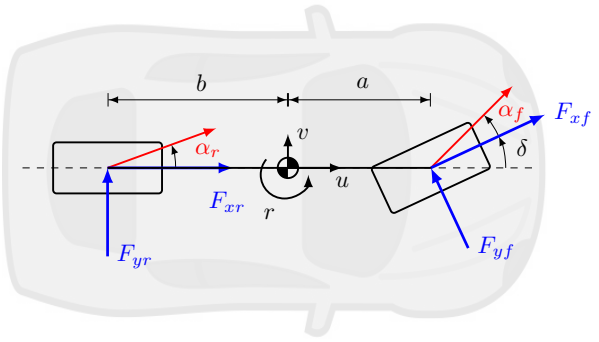


Figure 2. Diagram of the bicycle model.

The equations of motion are derived by analyzing the balance between forces and moments. From Figure 2, the lateral equations of motion are:

$$\begin{aligned} m(\dot{v} + ru) &= F_{yf}\cos\delta + F_{yr} - F_{xf}\sin\delta, \\ I_z\dot{r} &= a(F_{yf}\cos\delta + F_{xf}\sin\delta) - bF_{yr}, \end{aligned} \tag{1}$$

where $m$ and $I_z$ are the vehicle mass and yaw inertia, respectively. $F_{yi}$ and $F_{xi}$ are lateral and longitudinal forces and subscripts $i \in \{f, r\}$ denotes front and rear wheels. Constants $a$ and $b$ are the distances from the center of gravity to front and rear axles. $\delta$ is the front tire steer angle and $\alpha_i$ are the slip angles. Finally, $v$, $r$, and $u$ are the vehicle lateral, angular, and longitudinal speeds, respectively.

Assuming a constant longitudinal velocity $u_0$, a rear-wheel drive ($F_{xf} \approx 0$), model (1) is simplified to:

$$\begin{aligned} m(\dot{v} + ru_0) &= F_{yf}\cos\delta + F_{yr}, \\ I_z\dot{r} &= aF_{yf}\cos\delta - bF_{yr}. \end{aligned} \tag{2}$$

The main nonlinearities about (2) arise from the behavior of the forces. Several tire-ground interactions force models are shown in literature (Singh et al., 2018). In this paper, due to its simple and clear formulation, we choose the brush tire model (Pacejka, 2005). The reason for this choice is that it has few parameters compared to the traditional Pacejka's model and has the ability to capture the nonlinearity of the tire forces.

The bush model is mainly dependent on the slip angle $\alpha_i$. The slip angle is defined as the angle between the direction of motion and the wheel heading. From Figure 2 and considering the kinematics motion we have:

$$\begin{aligned} \alpha_f &= \frac{v + ar}{u_0} - \delta, \\ \alpha_r &= \frac{v - br}{u_0}. \end{aligned} \tag{3}$$

Following (Rajamani, 2011), the brush lateral tire force model is expressed as:

$$F_{yi} = \begin{cases} -\mu_i F_{zi}\text{sign}(\alpha_i), & \text{if } |\alpha_i| > \alpha_{sl_i}, \\ -2C_\alpha\sigma_y\{1 - |\theta_y\sigma_y| + \frac{1}{3}(\theta_y\sigma_y)^2\}, & \text{o/w}, \end{cases} \tag{4}$$

where $\alpha_{sl_i}$ is slip angle threshold needed to reach the full sliding condition, defined as:

$$\alpha_{sl_i} = \tan^{-1}\left(\frac{3\mu_i F_{zi}}{2C_\alpha}\right), \tag{5}$$

and with

$$\begin{aligned} \theta_y &= \frac{2C_\alpha}{3\mu_i F_{zi}}, \\ \sigma_y &= \tan\alpha_i, \end{aligned} \tag{6}$$

where $\mu_i$ are the available friction coefficient, $F_{zi}$ are the vertical forces, and $C_\alpha$ the cornering stiffness coefficient. Note that the factor $2C_\alpha$ in (4)-(6) accounts for the fact that we assume a lumped axle with twice the capacity of a single tire, i.e., the equivalence between the bicycle and the four-wheel planar model. Moreover, due to vehicle symmetry, we have equal front and rear cornering stiffness, therefore, $C_{\alpha f} = C_{\alpha r} = C_\alpha$.

For the vertical forces it is assumed the static load transfer:

$$\begin{aligned} F_{zf} &= bmg/(a+b), \\ F_{zr} &= amg/(a+b), \end{aligned} \tag{7}$$

where $g$ is the gravitational acceleration.

Substituting from (3), (4) and (7) into (2), we assemble the two complete equations describing the lateral dynamics with states $x = [v, r]^T$ and input $u = \delta$. For a comprehen-

sive analysis of the lateral vehicle model see (Rajamani, 2011, Chapter 2).

## 4. PARAMETER IDENTIFICATION

As seen in the previous section, the vehicle lateral behavior is strongly dependent on two fundamental parameters: tire cornering stiffness $C_\alpha$ and inertia $I_z$. When a sufficiently large dataset is considered, composed by measurements of states $v$ and $r$, it is possible to estimate the desired parameters using the analytical model described in Section 3. This methodology can be seen as a problem of fitting experimental data to a nonlinear analytical function.

The problem consists of finding the decision variables $x_p = [C_\alpha, I_z]^T$ that solve:

$$x_p^* = \arg\min_{x_p}(w_1 e_{v,rms} + w_2 e_{r,rms} + w_3 C_a + w_4 I_z) \quad (8)$$

subject to $C_a > 0$ and $I_z > 0$, where $x_p^* = [\hat{C}_\alpha, \hat{I}_z]^T$ is the optimum value that minimizes the objective function. Errors $e_{v,rms}$ and $e_{r,rms}$ are the states $v$ and $r$ $rms$ errors between the expected (measured) and simulated values. The positive constants $w_1 \dots w_4$ are the set of weighting factors that indicate the importance of the residuals. Problem 8 is optimized using the standard interior-point algorithm with BFGS hessian update implemented by the "fmincon" method in Matlab (Nocedal, 2006)

If experimental data were free of error, the parameters $C_\alpha$ and $I_z$ could be obtained straightforwardly by measuring the states at two points and solving the nonlinear model. Since it is not the case, a dataset should be used instead. Therefore, particular care must be taken in the data collection stage.

### *4.1 Data collection*

The estimated parameter accuracy in problem (8) is strongly dependent on the measured data (Xu and Zhai, 2019). To yield meaningful information about the vehicle lateral response we must gather a data set with a representative level of excitation. It can be achieved exciting the system with a swept sine wave input, also known as chirp signal. It is a persistently exciting signal used to disturb the system over a specified range of frequencies (Honorio et al., 2018).

In order to have a comprehensive and representative data set a number of tests must be performed. The test consists of applying constant longitudinal speed while employing the time-varying steer input in the vehicle of Figure 1. This process must be repeated for several steering angle amplitudes and different longitudinal speeds.

The dataset used in this work contains signals obtained varying the sine input amplitude from 10 to 25 degrees and by setting three constant longitudinal speeds: 0.25, 0.6, and 1 m/s. A total of 13658 measurements are gathered with a frequency of 10 Hz.

### *4.2 Comparative methods*

Here we propose comparing the estimation method (8) with two simpler approaches denoted '$a_y$-method' and '$\dot{r}$-method'. As discussed in (Sierra et al., 2006), these methods are intended to eliminate reliance on the measures of the vehicle states or its derivative. They are expressed by linearizing the vehicle model around a constant longitudinal velocity $u_0$ and is written as standard 1-norm minimization:

$$\arg\min_{C_\alpha} ||Ax - b||_1^2. \quad (9)$$

*$a_y$-method*

This method is based on the linearized lateral velocity dynamics:

$$F_y = ma_y = C_\alpha \alpha_f + C_\alpha \alpha_r. \quad (10)$$

Substituting (3) into (10), it is written as

$$\Big[\frac{v + ar}{u_0} - \delta + \frac{v - br}{u_0}\Big] C_\alpha = ma_y \quad (11)$$

which is in the standard regression form with $C_\alpha$ being the unknown. The drawbacks of this method are that it does not incorporate information about the inertia $I_z$, is strongly influenced by measurement noises, and requires persistent excitation.

*$\dot{r}$-method*

The fundamental equation of the $\dot{r}$-method is the linear approximation of (1):

$$I_z \dot{r} = aC_\alpha \alpha_f - bC_\alpha \alpha_r, \quad (12)$$

which can be rewritten as:

$$\Big[a\Big(\frac{v + ar}{u_0} - \delta\Big) - b\Big(\frac{v - br}{u_0}\Big)\Big] C_\alpha = I_z \dot{r}. \quad (13)$$

Note that it relies on the yaw derivative. During constant cornering $\dot{r}$ is zero and (13) will not perform properly. Additionally, $\dot{r}$ cannot be measured directly and must be band-pass filtered.

## 5. EXPERIMENTAL RESULTS

In this section, the performance of the parameter identification (8) method is verified using experimental data. Steering angle $\delta$ is measured by encoders, angular velocity $r$ is measured by the IMU and lateral velocity $v$ is filtered using the approach presented in (Moore and Stouch, 2014). The vehicle's main physical parameters required in this work are listed in Table 1.

Table 1. Vehicle physical parameters.

| **Parameter name (Symbol)** | **Value** |
|---|---|
| Vehicle mass (m) | 17.11 kg |
| Dist. from CG to front wheels (a) | 0.30 m |
| Dist. from CG to rear wheels (b) | 0.27 m |

As discussed in Section 4.1, the dataset is obtained by applying a swept sine input, also referred to as the chirp signal. The steering angle follows the chirp signal in an open-loop command and the experiment is repeated several times varying its amplitude and with different longitudinal speeds. A small fraction of this input contained in the dataset is shown in Figure 3. The wave starts with an initial frequency of 1 Hz and ends with 6 Hz.

Note that the imperfections of the sine wave are due to the experimental data nature. The steering angle, which follows the steering system dynamics, is achieved by an electric motor with a low-level position controller. Additionally, the first half-wave period is discarded due to initial measurement noises observed throughout the maneuver execution.

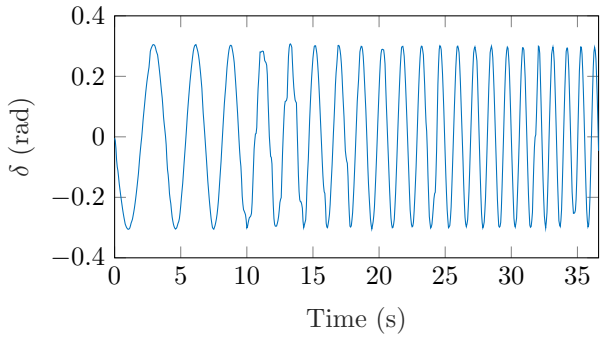


Figure 3. Steering angle following the swept sine signal. The first half period is discarded due to initial measurement noises.

The optimization problem (8) is solved via Matlab/Simulink in an off-board computer using the built-in "fmincon" function. Following an empirically trial and error approach, we chose $w_1 = 3$, $w_2 = 1$, $w_3 = 1 \times 10^{-7}$ and $w_4 = 2 \times 10^{-3}$. The weighting factors are chosen with respect to the magnitude and importance of the corresponding residuals.

Solving (8), the optimum estimated parameters obtained are $\hat{C}_\alpha = 94.75$ N and $\hat{I}_z = 1.64$ kg/m$^2$. Comparing with similar scaled vehicles found in literature, these values are consistent and strongly agrees (Sierra et al., 2006; Polley et al., 2006; Kozłowski, 2019).

On the other hand, evaluating the $a_y$-method and the $\dot{r}$-method by solving (9) we obtain $C_\alpha$ equal to 36.5407 and 74.53 N, respectively. Accordingly to (Sierra et al., 2006), the performance of these methods is significantly worse if compared to optimization (8) and the reason is simple, both methods rely on a single linearized equation. This makes the identified parameter extremely sensitive to noise measurement.

The comparative aforementioned methods are indicated when the experiment is evaluated at monitored workstations and test benches, where the noises can be measurable. Interestingly, the estimated values do not differ considerably from the optimum of (8), which indicates an appropriate and pertinent estimation. Therefore, our reference will be the value obtained solving the proposed problem (8).

To validate the estimated parameters, we propose a comparison between the simulated and experimental data. The simulated data were obtained via Matlab/Simulink by evaluating the nonlinear lateral model, described in Section 3, using the estimated parameters $\hat{C}_\alpha$ and $\hat{I}_z$.

### *5.1 Open loop scenario*

We first analyze the identified model considering the open-loop swept sine input of Figure 3. The vehicle is set with a constant longitudinal velocity of 0.25 m/s. Note that this scenario is contained in the data set used to estimate the desired parameters. Therefore, a satisfactory response should be expected.

The results are shown in Figure 4. It is notable the strong agreement between the measured and simulated vehicle states. The major discrepancy, observed in lateral velocity $v$, arises when increasing the input sine frequency. Despite that, the responses are in phase and the response time between both signals is consistent.

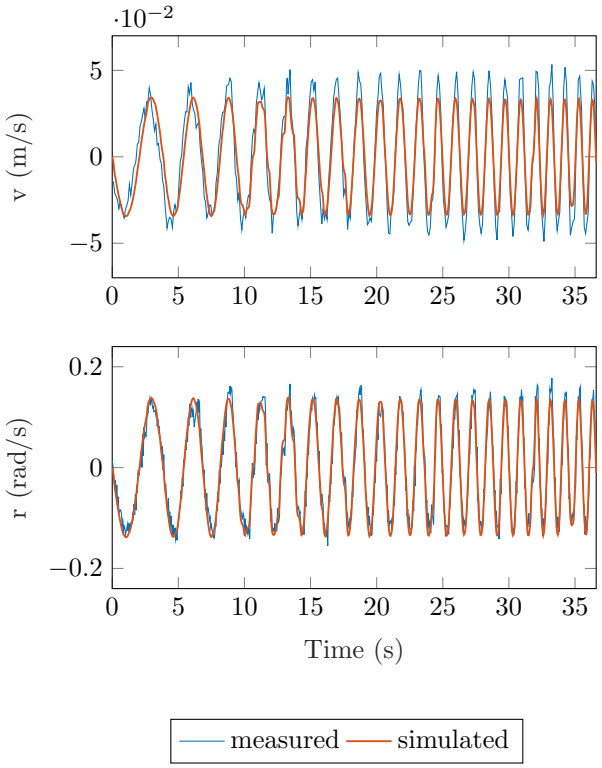


Figure 4. Estimated and measured vehicle lateral response for the open-loop sinusoidal input.

In Table 2 we show the states $v$ and $r$ *rms* errors for the three discussed methods. The scenario of Figure 4 is simulated using the estimated parameters of each approach and the errors are calculated between the expected and achieved response. In accordance with the former discussion, the performance of the proposed regression is slightly better. Therefore, the following results are presented with the parameters obtained by solving (8).

Table 2. Rms error of states $v$ and $r$ for the three proposed methods.

| **Method** | $e_{v,rms}$ | $e_{r,rms}$ |
|---|---|---|
| Regression (8) | 0.0112 | 0.0201 |
| $a_y$-method (11) | 0.0133 | 0.0273 |
| $\dot{r}$-method (13) | 0.0115 | 0.0209 |

*5.2 Closed loop scenario*

Now we wish to compare the estimated response with two practical maneuvers. The first is executed in an indoor environment with a perfectly planar surface. The second is performed in an outdoor environment, the ground surface has vertical irregularities and is composed of a mix of gravel and grass. The details are shown in the following sections.

*Indoor experiment*

The experiment was conducted with a constant linear speed of 0.4 m/s and setting two desired yaw rates of magnitudes 0.2 and -0.2 rad/s. This results in a maneuver where two circles with constant curvature radius are achieved with opposite directions.

The performed trajectory and the commanded steering angle $\delta$ are shown in Figures 5 and 6, respectively. The vehicle starts at the origin and executes the trajectory with a curvature radius of 2m. More details about this maneuver and its low-level control loop can be seen in (Nogueira et al., 2018).

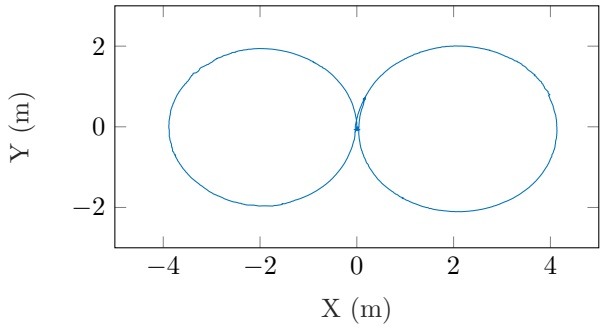


Figure 5. Performed trajectory of the proposed maneuver: two circles with constant 2m radius and opposite directions.

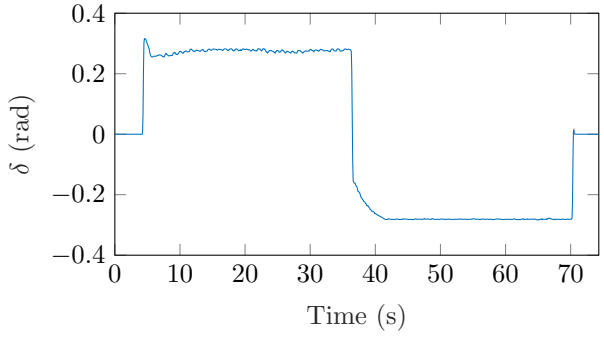


Figure 6. Commanded steering angle to keep the vehicle with the desired angular speed.

The lateral and angular velocities are shown in Figure 7. Note that $v$ cannot be measured directly. As discussed, it must be filtered and the quality of signal $v$ is associated with the measurement noises, such as lateral acceleration. Despite that, one can note a satisfactory agreement between the achieved and expected velocities obtained via simulation. This indicates that the optimization problem (8) is not overfitting the data.

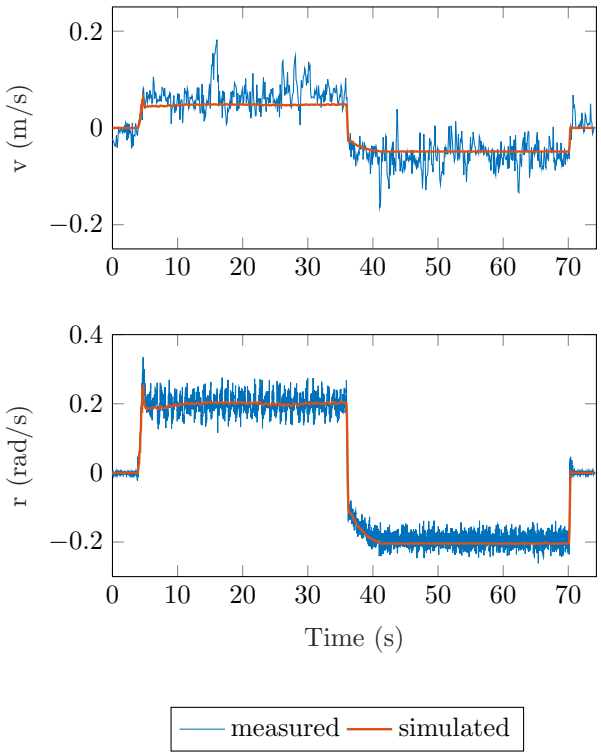


Figure 7. Actual and simulated vehicle response. On top and bottom are shown the lateral and angular velocities, respectively.

*Outdoor experiment*

The outdoor experiment consists of a closed-loop maneuver where the vehicle follows a desirable path. The vehicle autonomously travels through the center of an orchard row with a constant longitudinal speed of 1m/s.

The nature of this experiment is exposed in Figure 8 where the vehicle is oriented towards the orchard rows with an intentional initial lateral error.

Observe that, due to the trajectory nature, it is expected steering angle commands needed for the lateral error correction. More details about this maneuver and its high-level controller can be found in (de Lemos et al., 2018).

Figure 8. Platform in autonomous mode traversing the orchard corridor. The figure on left and right show the initial vehicle pose and after 10 seconds of execution, respectively.

The obtained vehicle trajectory and the commanded steering angle are shown in Figures 9 and 10, respectively. Note that the vehicle has an initial error of -1.12 m which leads to a high steering command effort, enforcing the initial lateral correction. After 10 seconds of execution,

the vehicle reaches the corridor center and the experiment follows with corrective steering angle commands of small magnitude.

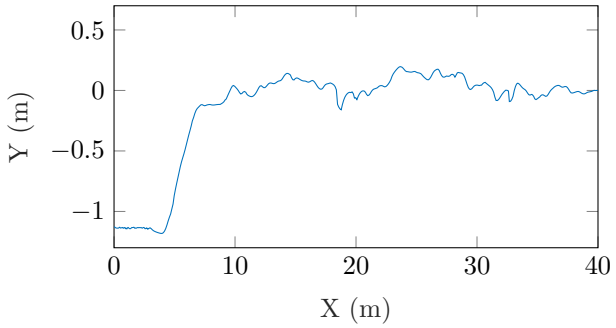


Figure 9. Performed trajectory with respect to the corridor center. The test begins with an intentional initial lateral error of -1.12 m.

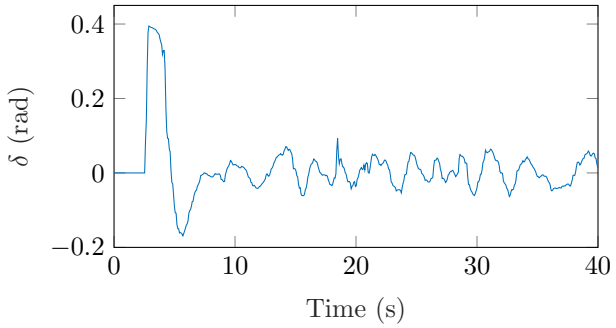


Figure 10. Commanded steering angle. The efforts at the initial instants are due to the lateral starting error.

Figure 11 shows the vehicle lateral response. For this experiment, unfortunately, we do not have access to the vehicle lateral velocity $v$. However, we can note a good agreement between the expected and achieved angular velocity $r$. Observe that, due to the outdoor environment and the associated ground irregularities, the measurement noise is strongly noticeable.

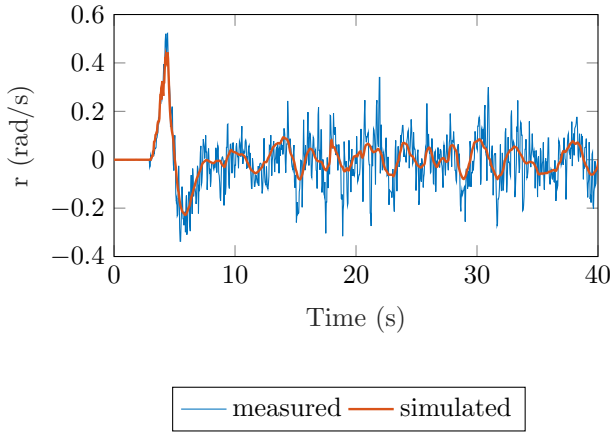


Figure 11. Measured and simulated angular velocity response for the outdoor experiment.

## 6. CONCLUSION

In this paper, we experimentally approached the vehicle parameter estimation. An optimization problem, based on the nonlinear vehicle lateral dynamic, is proposed. The main result is proper identification of the vehicle cornering stiffness coefficient and yaw moment of inertia. The motivation for this study is the capability of estimating the desired parameters using conventional sensors as an alternative to expensive workstations and test benches.

The proposed estimation process is a model-based approach that strongly relies on a set of measurements. Due to this characteristic, a wide variety of tests are needed in order to gather a comprehensive data set. The data collection stage is described and a persistently exciting signal is chosen to compose the dataset.

The proposed optimization problem was then solved with the experimental data and the estimated parameters are used to simulate the vehicle response. The estimation accuracy is verified by comparing the expected and achieve response for three representative scenarios. The resulting signals show an adequate agreement indicating that the proposed method was able to correctly estimate the desired parameters. Moreover, the identified values correspond to those presented in the literature for similar vehicles.

Efforts and future work will be concentrated at performing the parametric estimation in a real-time application, removing the off-board processing stage.

## ACKNOWLEDGMENT

The authors acknowledge the funding received from the FAPESP Regular project AutoVERDE N. 2018/04905-1, Ph.D. FAPESP 2018/05712-2, and Project INCT-SAC - Autonomous Collaborative Systems - (CNPq 465755/2014-3, FAPESP 2014/50851-0), FAPESP BEP (p. 2017/11423-0).

## REFERENCES

de Lemos, R.A., de O. Nogueira, L.A.C., Ribeiro, A.M., Mirisola, L.G.B., Koyama, M.F., de Paiva, E.C., and Bueno, S.S. (2018). Unisensory intra-row navigation strategy for orchards environments based on sensor laser. In *XXII Congresso Brasileiro de Automática*.

Denis, D., Nizard, A., Thuilot, B., and Lenain, R. (2015). Slip and cornering stiffnesses observation for the stability assessment of off-road vehicles. In *International Conference on Mediterranean Green Energy Forum*. Marrakech, Morocco.

Fnadi, M., Plumet, F., and Benamar, F. (2019). Nonlinear tire cornering stiffness observer for a double steering off-road mobile robot. In *2019 International Conference on Robotics and Automation (ICRA)*. IEEE.

Han, K., Choi, M., and Choi, S.B. (2018). Estimation of the tire cornering stiffness as a road surface classification indicator using understeering characteristics. *IEEE Transactions on Vehicular Technology*, 67(8), 6851–6860.

Honorio, L.M., Costa, E.B., Oliveira, E.J., de Almeida Fernandes, D., and Moreira, A.P.G. (2018). Persistently-exciting signal generation for optimal parameter estima-

tion of constrained nonlinear dynamical systems. *ISA Transactions*, 77, 231–241.

Kozłowski, M. (2019). Analysis of dynamics of a scaled PRT (personal rapid transit) vehicle. *Journal of Vibroengineering*, 21(5), 1426–1440.

Matsubara, M., Ishii, K., Kawamura, S., and Furukawa, T. (2019). Development of measurement system for deformation of the tire tread block using a digital camera. In *INTER-NOISE and NOISE-CON Congress and Conference Proceedings*, volume 260, 699–705. Institute of Noise Control Engineering.

Moore, T. and Stouch, D. (2014). A generalized extended kalman filter implementation for the robot operating system. In *Proceedings of the 13th International Conference on Intelligent Autonomous Systems (IAS-13)*. Springer.

Nocedal, J. (2006). *Numerical optimization*. Springer, New York.

Nogueira, L.A.C.O., Koyama, M.F., Cordeiro, R.A., Ribeiro, A.M., Bueno, S.S., and Bueno, S.S. (2018). A miniaturized four-wheel robotic vehicle for autonomous driving research in off-road scenarios. *XXII Congresso Brasileiro de Automática*.

Pacejka, H. (2005). *Tire and vehicle dynamics*. Elsevier.

Pinto, R., Velasquez, A.E.B., Pedraza, I.L.A., Higuti, V.A.H., Gasparino, M.V., and Becker, M. (2019). Deployment of a smooth clothoid-based path planningand predictive control for the autonomous navigationof a car-like robot. In *Proceedings of the 25th International Congress of Mechanical Engineering*. ABCM.

Polley, M., Alleyne, A., and Vries, E.D. (2006). Scaled vehicle tire characteristics: dimensionless analysis. *Vehicle System Dynamics*, 44(2), 87–105.

Rajamani, R. (2011). *Vehicle dynamics and control*. Springer Science & Business Media.

Sierra, C., Tseng, E., Jain, A., and Peng, H. (2006). Cornering stiffness estimation based on vehicle lateral dynamics. *Vehicle System Dynamics*, 44, 24–38.

Singh, K.B., Arat, M.A., and Taheri, S. (2018). Literature review and fundamental approaches for vehicle and tire state estimation. *Vehicle System Dynamics*, 57(11), 1643–1665.

Treetipsounthorn, K. and Phanomchoeng, G. (2018). Real-time rollover warning in tripped and un-tripped rollovers with a neural network. In *2018 IEEE 4th International Conference on Control Science and Systems Engineering (ICCSSE)*. IEEE.

Xu, L. and Zhai, W. (2019). A spectral evolution model for track geometric degradation in train–track long-term dynamics. *Vehicle System Dynamics*, 58(1), 1–27.

Yang, W., Guan, X., and Zhang, J. (2017). A recursive propagator-based subspace method for vehicle handling dynamic system model identification. *Proceedings of the Institution of Mechanical Engineers, Part D: Journal of Automobile Engineering*, 233(3), 495–516.

Zhang, N., Xiao, H., and Winner, H. (2015). A parameter identification method based on time–frequency analysis for time-varying vehicle dynamics. *Proceedings of the Institution of Mechanical Engineers, Part D: Journal of Automobile Engineering*, 230(1), 3–17.